# Photoionization of atomic barium subshells in the 4*d* threshold region using the relativistic multiconfiguration Tamm-Dancoff approximation

Aarthi Ganesan,[1] P. C. Deshmukh,[2,3] and S. T. Manson[4]
[1]*Department of Physics, Centre for Post-Graduate Studies, Jain University, Bengaluru 560011, India*
[2]*Department of Physics, Indian Institute of Technology Tirupati, Tirupati 517506, India*
[3]*Department of Physics, Indian Institute of Science Education and Research, Tirupati 517507, India*
[4]*Department of Physics and Astronomy, Georgia State University, Atlanta, Georgia 30303, USA*

(Received 9 December 2016; revised manuscript received 28 January 2017; published 17 March 2017)

Photoionization cross sections and photoelectron angular distribution asymmetry parameters are calculated for the $4d^{10}$, $5s^2$, $5p^6$, and $6s^2$ subshells of atomic barium as a test of the relativistic multiconfiguration Tamm-Dancoff (RMCTD) method. The shape resonance present in the near-threshold region of the 4*d* subshell is studied in detail in the 4*d* photoionization along with the 5*s*, 5*p*, and 6*s* subshells in the region of the 4*d* thresholds, as the 4*d* shape resonance strongly influences these subshells in its vicinity. The results are compared with available experiment and other many-body theoretical results in an effort to assess the capabilities of the RMCTD methodology. The electron correlations addressed in the RMCTD method give relatively good agreement with the experimental data, indicating that the important many-body correlations are included correctly.

DOI: 10.1103/PhysRevA.95.033417

## I. INTRODUCTION

The study of the photoionization atomic barium subshells has interested many over the last few decades [1–9]. Barium is an interesting many-body system to examine the combined effects of relativistic and correlation interactions, since (a) it is a high-$Z$ system so that relativistic (primarily spin-orbit) interactions play an important role, (b) the outer $6s^2$ subshell is known to be highly correlated, (c) the large photoionization cross section of the inner 4*d* subshell of barium, which undergoes a delayed maxima (shape resonance), strongly affects other nearby subshell cross sections *via* correlation in the form of interchannel coupling, and (d) sufficient experimental data [5–8] are available for atomic barium, with which theoretical results can be compared and assessed.

As is well known, the physics of the atomic photoionization process generally goes well beyond the description by the independent particle approximation since the many-electron correlations are important [10,11]. Even a nonrelativistic many-body theory is often inadequate. Among successful relativistic many-body methods, the relativistic random phase approximation (RRPA) [12] and the relativistic multiconfiguration Tamm-Dancoff (RMCTD) methods [13] include both relativistic and many-body correlation effects. The RRPA has been found to be quite successful in a number of different situations, for example, in the photoionization study of noble gas atoms [12–16], and several other closed-shell atoms from Groups IIA [17–19], IIB [20–22], and also Pd, Yb, Rd [23–25]. It has also been used with considerable success to account for photoionization of closed-shell negative ions. In addition, the RRPA has also been used along with the relativistic multichannel quantum defect theory [26] to understand autoionization resonances [27,28] in atomic systems. Notwithstanding the success of the RRPA method, it must be mentioned that even as it includes some of the most important electron correlations, the RRPA leaves out the correlations that come from the ionization-plus-excitation channels. The RMCTD method takes into account electron correlations in both the initial state and the final state of photoionization, like the RRPA, but differs from it in some details. Even as both RRPA and RMCTD take into account electron correlations in the final state *via* interchannel coupling, the initial-state correlations are included in the RRPA method by summing over all ring (and corresponding exchange) diagrams, whereas in the RMCTD method, the initial-state correlations are included *via* explicit configuration interaction by obtaining the initial-state wave functions using GRASP-92 [29] to generate multiconfiguration Dirac-Hartree-Fock (MCDHF) wave functions. This difference enables the application of the RMCTD method to take account of ionization-plus-excitation channels *not* included in the RRPA and from all the configurations which are explicitly included in the MCDHF wave function. Unfortunately, there are only a few studies in which the RMCTD method has been tested. For example, it has been used to account for photoionization of a very few atoms, Mg and Be [13], Cd [30], and Xe [31], and photodetachment of a few negative ions [32,33]. The present study tests the applicability of the RMCTD to a rather highly correlated atom, atomic barium. Salient features of the RMCTD method are reviewed in Sec. II below.

Various theoretical and experimental photoionization studies of atomic barium have been reported. On the experimental side, Bizau *et al.* [6] have reported x-ray photoelectron spectrometry (XPS) study of photoionization in atomic barium subshells using synchrotron radiation between 16 and 180 eV photon energy. Snell *et al.* [34] have measured the 4*d* and 5*p* photoelectron spectra of atomic barium using *narrow-bandwidth* synchrotron radiation of 131.2 eV photon energy. Whitfield *et al.* [8] have reported the angular distribution and the photoionization cross section of Ba 5*s* in the energy region of the second Cooper minimum, from 120 to 260 eV. The outer $6s^2$ subshell of Ba is very strongly mixed with $6p^2$ and $5d^2$, and hence single-particle calculations, e.g., Hartree-Fock (HF) and Dirac-Hartree-Fock (DHF), of the ground state are inadequate. Theoretical studies of atomic barium have been done using HF wave functions, both with and without relaxation, by Kelly *et al.* [4], the random phase approximation with exchange

(RPAE) [1], the RRPA [12], RRPA *with* relaxation (RRPA-R) [2], and many-body perturbation theory (MBPT) [3]. Kutzner *et al.* [3] have reported photoionization cross sections and angular distribution asymmetry parameters for inner and outer subshells of barium, including relaxation and polarization effects using MBPT. They used two different methods to include relaxation and polarization effects: one by taking into account the higher-order diagrams in MBPT and the other by calculating the excited-state wave functions in the potential of a relaxed ionic core. The MBPT results were found to be in good agreement with the available experimental data.

Thus, in contradistinction to the case of Xe [14], where methodologies like RRPA [12] work quite well, Ba requires far more in the way of correlation included to achieve quantitative accuracy, certainly more than is included in RRPA or RPAE, its nonrelativistic counterparts. This then offers an excellent case for the testing of the capabilities of the RMCTD method. In the present work, we focus on the photoionization in the energy region of the shape resonance in the $4d$ subshell cross section of atomic barium, where both initial- and final-state correlations are important. Non-RPA correlations are included in the present work by mixing other important configurations in the initial state using the RMCTD method. The dipole channels from the excited-state configurations to the continuum, along with the channels to the bound excited states, make this approach powerful to address electron correlations involved in the photoionization process. We report results using the RMCTD methodology and compare with results obtained using RRPA and RRPA-R methods, and also with available experimental data. Photoionizations from $4d$, $5s$, $5p$, and $6s$ subshells of barium are studied in the energy region in the neighborhood of the $4d$ thresholds.

## II. THEORY

The multiconfiguration initial-state wave function for RMCTD method is obtained using the General Purpose Relativistic Atomic Structure Program, GRASP92 [29]. GRASP92 is a suite of programs for calculating atomic energy levels, oscillator strengths, and discrete wave functions using a fully relativistic approach. The radial charge density of the nucleus is calculated based on the Fermi statistical distribution function. The $\alpha$th atomic state function (ASF) for an $N$-electron system is a linear combination of the $n_c$ number of electronic configuration state functions (CSFs) [35], expressed as $\Psi_\alpha^{\mathrm{PJM}} = \sum_{i=1}^{n_c} C_{i\alpha}\Phi_i^{\mathrm{PJM}}$,where $P$ (parity), $J$, and $M$ (total and azimuthal angular momenta) are symmetry labels. The CSFs ($\Phi_i^{\mathrm{PJM}}$) are linear combinations of $N$-electron Slater determinants made up of the four-component bispinors, $N$ being the number of initial-state electrons. The *five* explicit configurations included in the present work to describe the initial state are shown in Table I.

The first configuration is the usual HF or DHF ground state, and the other configurations are built on it by considering two-electron excitations from 6s to $5d$ or the $6p$ subshells. The configuration mixing weight factor obtained from the MCDHF formalism for each configuration is indicated above in Table I.

TABLE I. Initial-state configurations included in the present work.

| Initial-state configurations included | Weight factor |
|---|---|
| (1) $[\mathrm{Xe}]6s_{1/2}{}^2$ | $a_1 = 0.964$ |
| (2) $[\mathrm{Xe}]6s_{1/2}{}^0 5d_{3/2}{}^2$ | $a_2 = 0.067$ |
| (3) $[\mathrm{Xe}]6s_{1/2}{}^0 5d_{5/2}{}^2$ | $a_3 = 0.080$ |
| (4) $[\mathrm{Xe}]6s_{1/2}{}^0 6p_{1/2}{}^2$ | $a_4 = 0.117$ |
| (5) $[\mathrm{Xe}]6s_{1/2}{}^0 6p_{3/2}{}^2$ | $a_5 = 0.211$ |

The application of an external time-dependent harmonic perturbation $v_+ e^{-i\omega t}$ perturbs the MCDHF wave function. The external perturbation used in the RRPA included positive and negative frequency terms, while in RMCTD only the positive frequency term is used. The continuum orbital function $\bar{y}_a$ for a channel $a \to \bar{a}$ is the solution of the following radial integro-differential equation [13]:

$$(h_{\bar{a}} + V_{\bar{a}} + \varepsilon_a - \omega) y_{\bar{a}} = R_{\bar{a}}, \tag{1}$$

where $h_{\bar{a}}$ is the radial free-particle Dirac Hamiltonian, $V_{\bar{a}}$ is the Hartree-Fock $V(N-1)$ potential, $\varepsilon_a$ is the eigenvalue of the ground-state orbital (hole) $a$, and $\omega$ is the photon energy. The inhomogeneous term $R_{\bar{a}}$ describes the interchannel coupling and can be written as

$$R_{\bar{a}} = C_{\bar{a}} + B_{\bar{a}} + L_{\bar{a}}, \tag{2}$$

where $C_{\bar{a}}$ describes the coupling between channels, $B_{\bar{a}}$ describes the coupling with transitions $b \to b'$ between valence orbitals leading to excited-bound (XB) states, and $L_{\bar{a}}$ is the term with Lagrange multipliers, ensuring the orthogonality to the ground-state orbitals.

For the multichannel RMCTD excited-state wave function with total angular momentum $J$, $M$ has the form [13,33] expressed as

$$\psi(JM) = \sum_{i=1}^{n_c} c_i \chi(\gamma_i JM) + \sum_{\ell=1}^{n_b} b_\ell \Phi(\gamma_\ell JM), \tag{3}$$

where $\chi(\gamma_i JM)$ and $\Phi(\gamma_\ell JM)$ are configuration wave functions obtained from one of the initial-state configurations ("parent" configuration) by photoexciting a valence orbital (hole $a$) to a continuum orbital $\bar{a}$ or to another initial vacant state (valence) orbital, respectively. $\gamma_i$ and $\gamma_j$ represent all other quantum numbers required to define the corresponding configurations uniquely. The parameters $c_i$ and $b_\ell$ are the weight coefficients of the parent configuration and XB configuration composed of ground-state orbitals. $nc$ and $nb$ are the number of the continuum and excited-bound configurations, respectively. The weight coefficient $b_\ell$ corresponding to the XB configuration is obtained by solving the system of equations

$$\sum_{\ell=1}^{n_b} [H_{k\ell} - (E_0 + \omega)\delta_{k\ell}] b_\ell = F_k, k = 1,2,\ldots.,n_b, \tag{4}$$

where $H_{k\ell}$ is the atomic Hamiltonian matrix element $\langle \Phi(\gamma_k JM)|H|\Phi(\gamma_\ell JM)\rangle$ between two XB configurations $k$ and $\ell$, and $F_k$ corresponds to the matrix element between the XB configuration $k$ and the configuration corresponding to continuum channel $I$, which is expressed as

$$F_k = -\sum_{i=1}^{n_c} H_{ki} c_i, \tag{5}$$

TABLE II. Dirac-Hartree-Fock, $\Delta E_{\mathrm{SCF}}$, and MCDHF thresholds in eV along with available experiment.

| Subshell | DHF | $\Delta E_{\mathrm{SCF}}$ | MCDHF | Experiment [6,36] |
|---|---|---|---|---|
| $4s_{1/2}$ | 279.11 | 272.348 | 278.90 | |
| $4p_{1/2}$ | 220.37 | 213.773 | 220.16 | |
| $4p_{3/2}$ | 204.43 | 198.102 | 204.23 | |
| $4d_{3/2}$ | 106.49 | 100.59 | 106.29 | 101.02 |
| $4d_{5/2}$ | 103.75 | 97.94 | 103.54 | 98.41 |
| $5s_{1/2}$ | 43.63 | 41.824 | 43.45 | 38.06 |
| $5p_{1/2}$ | 26.03 | 24.312 | 25.85 | 24.75 |
| $5p_{3/2}$ | 23.75 | 22.138 | 23.58 | 22.72 |
| $6s_{1/2}$ | 4.44 | 4.28 | 4.99 | 5.21 |

where $H_{ki} = \langle \chi(\gamma_k JM)|H|\chi(\gamma_i JM)\rangle$. In Eq. (4), $E_0$ is the ground-state energy and $\omega$ is the photon energy.

Table II gives the ionization threshold energies calculated from DHF, ΔESCF, and MCDHF (GRASP92) which are used for RRPA, RRPA-R, and RMCTD, respectively.

Tables III and IV list the ionization and excitation channels used in the present calculations. Including dipole channels from the inner subshells from all the configurations involved in the configuration interaction improves the agreement between the theory and the experiment. There are 78 bound-to-continuum relativistic dipole ionization channels arising from the $4d + 5s + 5p + 6s + 5d + 6p$ subshells, and, in addition, there are nine bound-to-bound excitation channels. Thus, in the present work, interchannel coupling between a total of 87 channels is included.

With reference to Tables III and IV, the advantages of the RMCTD method over other many-body methods are explained in detail below. In Table III, the six allowed dipole channels from the spin-orbit split $4d$ subshells are listed. In the RRPA, we could consider only these six channels from the $4d$ subshells. The RMCTD method enables the inclusion of all relativistic dipole channels from all the five explicit configurations listed in Table I. This adds up to 15 channels for the $4d$ subshell as opposed to the six channels from $4d$ included in the RRPA. Also, the excitation channels from $5p$ and $6s$ are included in the RMCTD method. As discussed, the RMCTD method is formulated to include ionization channels from the excited-state configuration, in addition to the channels from the parent configuration. In order to understand the effects due to configuration interaction, we have done two sets of RMCTD calculations in the present work: (a) all dipole channels only from the first configuration listed in Table I, and (b) all dipole channels from all the five MCDHF configurations specified in Table I. Set (a) leads to interchannel coupling between 31 photoionization dipole channels (26 channels from bound-to-continuum states and five channels from bound-to-excited-bound states). When all the dipole channels from the five configurations listed in Table I are considered (set b), we get interchannel coupling between 87 dipole channels, listed in Tables III and IV. Inclusion of these additional channels improves agreement with the experiment, as shown in Sec. III.

TABLE III. Bound-to-continuum channels.

| $n \to \varepsilon$ channels | Initial-state configuration number | Number of channels (Total: 78) |
|---|---|---|
| $4d_{3/2} \to p_{1/2}, p_{3/2}, f_{5/2}$ | 1, 2, 3, 4, 5 | 15 |
| $4d_{5/2} \to p_{3/2}, f_{5/2}, f_{7/2}$ | 1, 2, 3, 4, 5 | 15 |
| $5s \to p_{1/2}, p_{3/2}$ | 1, 2, 3, 4, 5 | 10 |
| $5p_{1/2} \to s_{1/2}, d_{3/2}$ | 1, 2, 3, 4, 5 | 10 |
| $5p_{3/2} \to s_{1/2}, d_{3/2}, d_{5/2}$ | 1, 2, 3, 4, 5 | 15 |
| $6s \to p_{1/2}, p_{3/2}$ | 1 | 2 |
| $5d_{3/2} \to p_{1/2}, p_{3/2}, f_{5/2}$ | 2 | 3 |
| $5d_{5/2} \to p_{3/2}, f_{5/2}, f_{7/2}$ | 3 | 3 |
| $6p_{1/2} \to s_{1/2}, d_{3/2}$ | 4 | 2 |
| $6p_{3/2} \to s_{1/2}, d_{3/2}, d_{5/2}$ | 5 | 3 |

TABLE IV. Bound-to-bound channels.

| Initial-state configuration number | $n \to n'$ channels | Number of channels (Total: 09) |
|---|---|---|
| 1 | $5p_{1/2} \to 5d_{3/2}$ | 5 |
| | $5p_{3/2} \to 5d_{3/2}, 5d_{5/2}$ | |
| | $6s \to 6p_{1/2}, 6p_{3/2}$ | |
| 4 | $5p_{1/2} \to 6s_{1/2}$ | 2 |
| | $5p_{3/2} \to 6s_{1/2}$ | |
| 5 | $5p_{1/2} \to 6s_{1/2}$ | 2 |
| | $5p_{3/2} \to 6s_{1/2}$ | |

In the present work, we report the RMCTD results of the photoionization cross section and the photoelectron angular distribution asymmetry parameters for photoionization from various subshells of atomic barium. The relativistic electric dipole photoionization cross section is given, for the $i$th (or $l$th) configuration, by [12,37]

$$\sigma_{n\kappa}^{(i,\ell)}(\omega) = \frac{4\pi^2\alpha}{3}\omega\left(\left|D_{j\to j-1}\right|^2 + \left|D_{j\to j}\right|^2 + \left|D_{j\to j+1}\right|^2\right), \tag{6}$$

with the net cross section being the weighted sum of the contributions from each configuration,

$$\sigma_{n\kappa} = \sum_{i=1}^{n_c} {c_i}^2 \sigma_{n\kappa}^{(i)} + \sum_{\ell=1}^{n_b} {b_\ell}^2 \sigma_{n\kappa}^{(\ell)}, \tag{7}$$

where the coefficients $c_i$ and $b_\ell$ are from Eq. (3), above. Here, $\alpha$ is the fine-structure constant, $\omega$ is the photon energy, and the $D's$ are the dipole matrix elements given by $D_{nj\to j'} = i^{1-l} e^{i\delta_k} \langle \kappa || Q_1^{(1)} || \kappa_b \rangle$ (explained in Ref. [12]) for the various possible $j \to j'$ transitions allowed by dipole selection rules. The angular distribution asymmetry parameter is given, for the

$i$th (or $l$th) configuration, by [12]

$$\beta_{n\kappa}^{(i,\ell)}(\omega)=\frac{\begin{bmatrix}\frac{(2j-3)}{2(2j)}\left|D_{j\to j-1}\right|^2-\frac{(2j-1)(2j+3)}{(2j)(2j+2)}\left|D_{j\to j}\right|^2+\frac{(2j+5)}{2(2j+2)}\left|D_{j\to j+1}\right|^2\\ -\frac{3}{2j}\left(\frac{(2j-1)}{2(2j+2)}\right)^{\frac{1}{2}}(D_{j\to j-1}D^{*}_{j\to j}+\mathrm{c.c})-\frac{3}{2}\left(\frac{(2j-1)(2j+3)}{(2j)(2j+2)}\right)^{\frac{1}{2}}(D_{j\to j-1}D^{*}_{j\to j+1}+\mathrm{c.c})\\ +\frac{3}{(2j+2)}\left(\frac{(2j+3)}{2(2j)}\right)^{\frac{1}{2}}(D_{j\to j}D^{*}_{j\to j+1}+\mathrm{c.c})\end{bmatrix}}{|D_{j\to j-1}|^2+|D_{j\to j}|^2+|D_{j\to j+1}|^2},\tag{8}$$

with the net $\beta_{n\kappa}(\omega)$ for each subshell being given by $\beta_{n\kappa}(\omega)=\frac{\sum_{i=1}^{n_c}{c_i}^2\sigma_{n\kappa}^{(i)}\beta_{n\kappa}^{(i)}+\sum_{j=1}^{n_b}{b_j}^2\sigma_{n\kappa}^{(j)}\beta_{n\kappa}^{(j)}}{\sum_{i=1}^{n_c}{c_i}^2\sigma_{n\kappa}^{(i)}+\sum_{j=1}^{n_b}{b_j}^2\sigma_{n\kappa}^{(j)}}$.

## III. RESULTS AND DISCUSSION

The RRPA and RRPA-R calculations reported earlier [2] were repeated and reproduced first as a check, with a small difference in that we included additional channels from the 4s and 4p subshells, in addition to those from the $4d$, $5s$, $5p$, and $6s$ subshells employed earlier [2]. The addition of the $4s+4p$ channels does not, however, have any significant impact on the photoionization parameters of the $4d$ subshell. The RRPA and the RRPA-R results presented in this work include all relativistic dipole channels from $4s$, $4p$, $4d$, $5s$, $5p$, and $6s$ subshells. The photoionization cross sections and the photoelectron angular distributions presented in the figures below are from the set b calculation of RMCTD method, as mentioned in Sec. II. In this work, we report photoionization cross sections of the $4d$ subshell and also of the $6s$, $5p$ and $5s$ subshells of atomic barium in the energy region in the neighborhood of the $4d$ ionization threshold. In addition, we present photoelectron angular distributions of the $4d$ and $5p$ photoelectrons.

### A. 4*d* subshell

The enhancement in the photoionization cross section due to the giant (shape) resonance [38] in the $4d$ subshell strongly influences the matrix elements for photoionization of other subshells in the energy region near the $4d$ delayed maximum *via* interchannel coupling. Kelly *et al.* [4] have calculated the photoionization cross section of a barium $4d$ subshell at the HF level, both with and without the inclusion of relaxation effects, and found that the presence of relaxation effects broadened the peak in the $4d$ cross section (Fig 1). The RPAE photoionization cross section [1] in the near-threshold region for the $4d$ subshell overestimates the experimental cross section [5–7,39] by about 60 Mb; RRPA brings the peak cross section down (relative to RPAE), but nevertheless 25 Mb higher than the experimental data. Including relaxation effects, in addition to the relativistic effects (RRPA-R), the cross section is reduced further, getting close to the experimental value [2]; the remaining difference from experiment is probably due to the omission of double electron excitations in the calculation.

The $4d$ photoionization cross section for barium is considerably more sensitive to the inclusion of relativistic, relaxation, and interchannel coupling effects compared to that for xenon, which is different from barium only in the absence of the $6s$ electrons [2]. This has been explained [2] in terms of the extraordinary sensitivity of the double-well effective potential for an $f$ electron excited from the $4d$ subshell in Ba compared to Xe. In the case of atomic barium, the $f$ electron is on the verge of being able to bind in the inner well as in the lanthanides. This, of course, makes the $4d\to f$ shape resonance in Ba very sensitive, since small changes in the potential alter the presence of $f$ electrons in one or the other potential well and, in turn, strongly affects the energy dependence of the photoionization cross section. The results of the various calculations for the Ba $4d$ photoionization cross section are shown in Fig. 1, where it is seen that the RMCTD [geometric mean (GM) of length and velocity] results are in reasonable agreement with experiment. It is clear that mixing the $6s^2$ outer-shell configuration with $5d^2$ and $6p^2$ excited state diminishes the value of the $4d$ cross section to a considerable amount compared to RPAE, RRPA, and the RRPA-R, and brings the result into much better agreement with experiment. Results are presented on the photoelectron energy scale since the ionization thresholds obtained from the DHF, $\Delta E_{\mathrm{SCF}}$, and GRASP-92 methods are different. The *total* $4d$ cross section presented is the sum of the $4d_{3/2}$ and $4d_{5/2}$ cross sections.

From the comparison it is clear that most of the methodologies predict a $4d$ cross section that is too large, sometimes

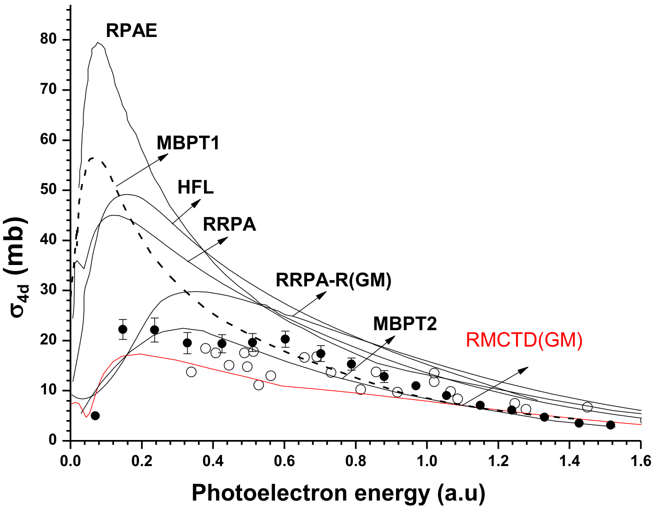

FIG. 1. Ba $4d$ photoionization cross section vs photoelectron energy. Theoretical results shown are the geometric mean of the present RMCTD results, labeled RMCTD (GM), along with RPAE [1], HF-length (HFL) [4], RRPA [2], the geometric mean of RRPA with relaxation, RRPA-R (GM) [2], and the length forms of MBPT [3] without relaxation (MBPT1) and with relaxation and polarization (MBPT2). The solid circles are the experimental results of Ref. [5], and open circles are from Ref. [6].

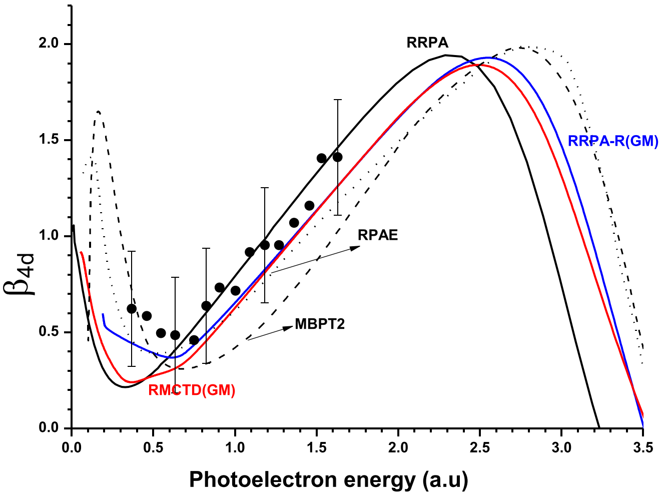

FIG. 2. Ba 4$d$ photoelectron angular distribution $\beta$ parameter shown along with various theoretical results. Shown are the present RMCTD, which is the geometric mean of length and velocity forms, denoted as RMCTD (GM), RPAE [1], MBPT2, which includes relaxation and polarization effects [3], RRPA, and RRPA-R (GM), which are the results of the present work, as described in the text.

grossly, e.g., the maximum in the RPAE cross section is a factor of 4 larger than experiment. The cross section is lowered by the introduction of relativistic effects; the RRPA result is half of the RPAE cross section. Relaxation, interchannel coupling, and initial-state correlation all seem to be of some importance. It is of interest to note that the MBPT2 (The MBPT calculation that includes relaxation and polarization effects) [3] also gives reasonably good agreement with experiment, despite being entirely nonrelativistic. It is to be noted that and RPAE-based calculation that included core rearrangement and relaxation [1] (not shown) also gave reasonable agreement with experiment, even though it, too, was nonrelativistic. In any case, however, the RMCTD (GM) methodology apparently contains all of the important physics to reproduce the experimental cross section in a satisfactory manner.

The angular distribution asymmetry parameter $\beta_{4d}$ is presented in Fig. 2 for RRPA, the RRPA-R, and the RMCTD methods. For a spin-orbit-split $nl$ shell, $\beta_{nl}$ is the weighted average [12] $\beta_{nl} = \frac{\sum_\kappa \sigma_{n\kappa}\beta_{n\kappa}}{\sum_\kappa \sigma_{n\kappa}}$; for the 4$d$ subshell, we have $\beta_{4d} = \frac{\sigma_{4d_{3/2}}\beta_{4d_{3/2}}+\sigma_{4d_{5/2}}\beta_{4d_{5/2}}}{\sigma_{4d_{3/2}}+\sigma_{4d_{5/2}}}$. Above the threshold region, all the theories are in reasonably good agreement with the experimental data. The length and velocity form (not shown individually) are fairly close to each other in RMCTD method.

Unlike the case of the cross sections, all of the theoretical results for $\beta$ are in rather good agreement with each other, and also with experiment, except for some differences near the threshold. $\beta$ is determined by the ratio of the magnitudes of the $4d \rightarrow f$ and $4p \rightarrow d$ matrix elements, along with the phase difference of the matrix elements [40]. The RPAE and the present RMCTD (GM) results for the photoelectron angular distribution parameter are in relatively good agreement compared to the comparison of the corresponding cross sections. This is presumably because of the fact that the photoelectron angular distribution asymmetry parameter is given by a ratio in which the differences in the cross section get cancelled out.

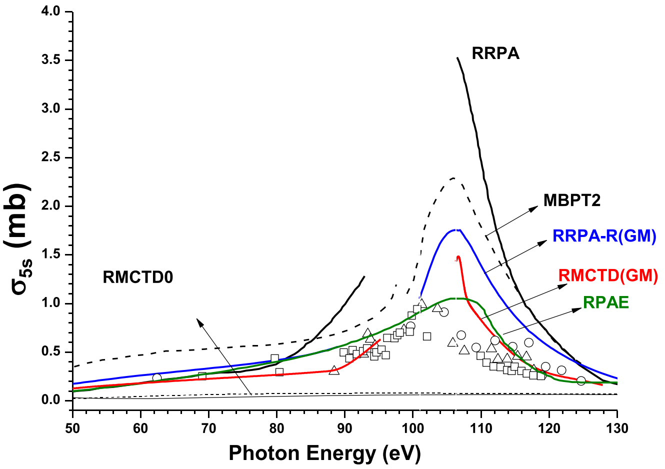

FIG. 3. Ba 5$s$ photoionization cross section in the region of the 4$d$ thresholds. The theoretical curves are labeled as in Fig. 1, with the addition of the RMCDT0 results in which the coupling with the 4$d$ photoionization channels is omitted in length (solid line) and velocity (dashed line) formulations, and RPAE-R, which is RPAE with the addition of rearrangement and relaxation [41]. The discontinuities in the theoretical curves are owing to the omission of the regions of autoionizing resonances below the 4$d$ thresholds, which have been left out to simplify the comparisons. The theoretical curves are shifted by the difference between the theoretical and experimental $4d_{3/2}$ thresholds. The experimental results shown are open circles [5], open triangles [6], and open squares [42].

### B. 5$s$, 5$p$, and 6$s$ subshells

The Ba 5$s$ photoionization cross section, shown in Fig. 3, is very strongly affected by correlation, specifically, correlation in the form of interchannel coupling [43,44] with the 4$d$ photoionization channels. To fully appreciate the dramatic effect of the correlation, the RMCTD length and velocity cross sections were also determined *without* coupling the 4$d$ photoionization channels. The results, without the 4d channels coupled, are labeled in Fig. 3 as RMCTD0, and are found to be very tiny over the entire range of energies, no more than a few hundredths of a Mb. With the coupling, however, the RMCTD result is seen to be almost 2 orders of magnitude larger. In other words, the single-particle cross section is essentially irrelevant, in this case, and the Ba 5$s$ cross section is completely dominated by interchannel coupling with the 4$d$ channels. And it is also clear from Fig. 3 that the RMCTD (GM) cross section is in reasonable quantitative agreement with experiment, which the RRPA, MBPT, and RRPA-R are not. Note that in Fig. 3, for purposes of comparison, the various theoretical curves have been shifted horizontally to match their $4d_{3/2}$ threshold (or 4$d$ for nonrelativistic calculations) with the experimental $4d_{3/2}$ threshold. The discontinuities in the theoretical curves are the autoionization regions, which are omitted in the plot to simplify comparison. Note further that the RPAE-R result, which is RPAE plus rearrangement and relaxation taken into account, exhibits quite good agreement with experiment, even though it is nonrelativistic.

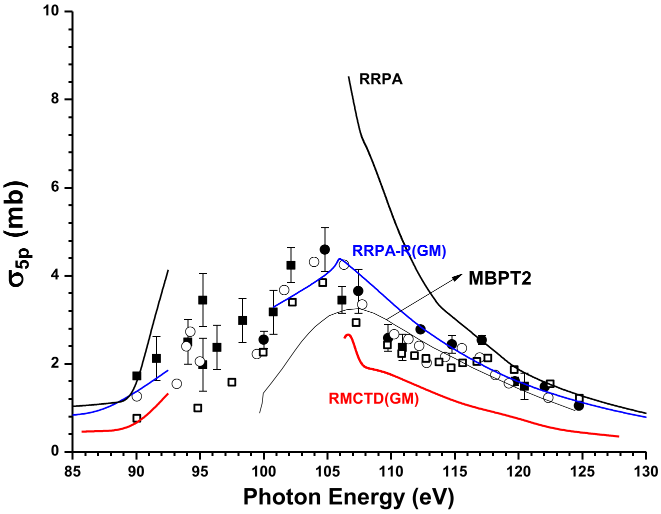

FIG. 4. Ba $5p$ photoionization cross section. The theoretical curves are labeled as in Fig. 1, with the discontinuities leaving out the autoionization resonances. Experiment is given by closed squares [6], closed circles [5], and open circles [42]. The theoretical curves are shifted by the difference between the theoretical and experimental $4d_{3/2}$ thresholds.

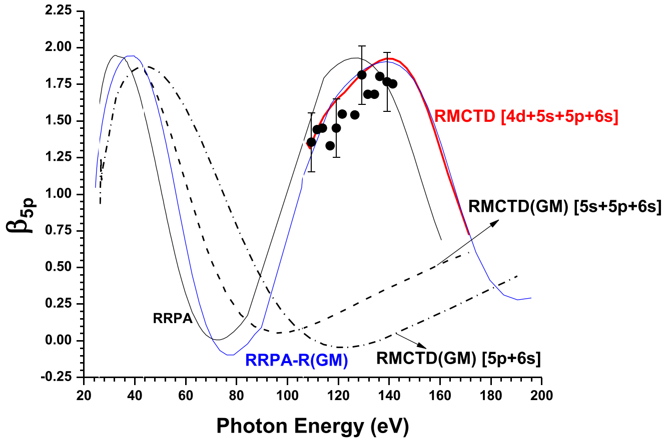

FIG. 5. Ba $5p$ photoelectron angular distribution parameter $\beta$ with the theoretical curves labeled as in Fig. 1, except that the RMCTD (GM) results are shown for several different levels on truncation, as indicated. The experimental values are from Ref. [5].

The calculated RMCTD $5p$ photoionization cross section, the sum of the $5p_{1/2}$ and $5p_{3/2}$ cross sections, is shown in Fig. 4 along with the results of several other calculations and experiment. As with the $5s$, the $5p$ cross section is dominated by the interchannel coupling with $4d$ photoionization channels. The experimental data is seen to be a bit scattered, e.g., at around 95 eV the highest experimental point is a factor of 3 larger than the smallest, well outside the stated error bars. Owing to this experimental scatter, it is difficult to assess the RMCTD results fully, but they are seen to be in the right ballpark. Better experimental data here would be most useful. In any case, the RRPA-R (GM) seems to give the best agreement with experiment, slightly better than RMCTD (GM), which seems to indicate that not all important initial-state correlations have been taken into account in RMCTD.

The angular distribution asymmetry parameter $\beta$ for the $5p$ subshell obtained from the RRPA, RRPA-R, and the RMCTD methods is shown in Fig. 5. The $\beta$ for the spin-orbit split $np$ subshell is calculated exactly as described for the $4d\beta$ case, i.e., by taking a weighted average of the asymmetry parameters of $p_{1/2}$ and $p_{3/2}$ subshells. The RRPA and RRPA-R calculations are done by including all dipole channels from the $4s + 4p + 4d + 5s + 5p + 6s$ subshells. Results are presented at different levels of truncation of RMCTD method. In all the theories, we note that interchannel coupling with channels from the $4d$ subshell is necessary to get agreement with the experiment, results which omit that coupling disagrees with experiment strongly. Thus the RMCTD results in which coupling with $4d$ channels is omitted is not in good agreement with experiment, whereas the RMCTD calculation inclusive of $4d$ coupling is in good agreement. We observe that the agreement between theory and experiment for the angular distribution asymmetry parameter is somewhat better in the case of $4d$ photoionization compared to that of $5p$. The $4d\beta$ is determined by the interference between $d \rightarrow f$ and $d \rightarrow p$ channels, and the relative strength is strongly in favor of the $d \rightarrow f$ channels. In the case of the $5p\beta$, which is determined by the interference between $p \rightarrow d$ and $p \rightarrow s$, the relative strength of the $p \rightarrow d$ channels is comparably not that much stronger than the $p \rightarrow s$ channel, as is the case with $4d\beta$. Therefore any neglect of detailed correlation is of less importance in the case of $4d\beta$ compared to $5p\beta$.

The length and velocity forms of the RMCTD method are fairly close to each other. The geometric mean of the two forms is given for the RRPA-R and RMCTD methods in Fig. 5. The RMCTD calculation of $\beta$ is in very good agreement with the experiment, which means that the relative phases of the various partial waves are accurate, and that the Cooper minimum is at the correct location. Again, it would be good to experiment over a broader range of energies for a more extensive comparison to test theory.

The RMCTD Ba $6s$ photoionization cross section is shown in Fig. 6 along with several other theoretical results and

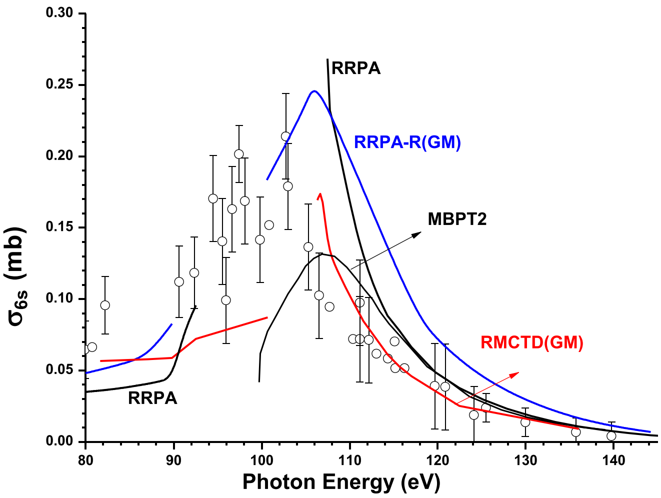

FIG. 6. Ba $6s$ photoionization cross section. Theoretical curves as Fig. 1, experiment, Ref. [6]. The theoretical curves are shifted by the difference between the theoretical and experimental $4d_{3/2}$ thresholds.

experiments. The cross section is quite small, maximizing at less than 0.2 Mb in this energy region; however, it is much larger than the cross section calculated without coupling with the $4d$ photoionization channels. Thus, as in the cases of $5s$ and $5p$, the maximum in the cross section in the 100-eV region is entirely due to interchannel coupling with the $4d$ channels. Also, as in the previous cases, the calculations are entirely *ab initio*, except for a shift in energy so that the calculated $4d_{3/2}$ threshold aligns with the experimental. The RMCTD (GM) cross section is in rather good agreement with experiment, especially in the higher-energy region, and the overall agreement with experiment is better than the RRPA, RRPA-R, or MBPT results, as seen in Fig. 6. It must be pointed out, however, that the experimental results exhibit significant scatter and large error bars; more accurate experimental data would be most helpful in assessing theory.

## IV. CONCLUSIONS

Analysis of the photoionization of atomic Ba is a challenging problem on account of the many-electron correlations which contribute to the details of its experimental features. Unlike the Xe atom [14] for which the RRPA results are in quite good agreement with experiment for $4d$ photoionization, the RRPA results for Ba overestimated the experimental cross sections [2]. The present RMCTD results, which include non-RPA correlations from the use of a MCDHF initial-state wave function and various dipole ionization and excitation channels originating from the multiconfigurational initial state, provides the best agreement with the available experimental data in the following cases: (a) the $4d$ cross section (with respect to the experimental results of Bizau *et al.* [6], although the MBPT results agree better with the experimental results of Becker *et al.* [5]), even as both RMCTD and the MBPT results give good agreement at higher energies with both sets of experimental data; (b) the $5s$ cross section in the energy region below the $4d$ threshold, as well as in the energy region well above the $4d$ threshold; and (c) the $6s$ cross section above the $4d$ threshold. The RMCTD results for the photoelectron angular distribution asymmetry parameters $\beta$ are also in best agreement with experimental data compared to other theoretical models in the following cases: (a) the $4d\beta$, although RRPA-R gives equally good agreement, and (b) the $5p\beta$ above the $4d$ threshold. In the case of some other features of the spectra, some of the other theoretical models give somewhat better agreement with the experiment. For example, the RPAE-R gives the best agreement with regard to the $4d$ cross section at its threshold. Overall, however, RMCTD results are in best agreement with the data in the largest number of cases.

The present work demonstrates the utility of the RMCTD method in various applications and projects it as a competitive relativistic, many-body methodology for the analysis of atomic photoionization processes. An added advantage which the RMCTD method has above the RPA/RRPA methods is the fact that it can also be used to study open-shell atoms and ions, since both the multiconfiguration expansion of the initial-state wave functions and the Tamm-Dancoff multichannel final-state wave functions are admissible in the RMCTD method.

## ACKNOWLEDGMENTS

The work of S.T.M. was supported in part by the U.S. Department of Energy, Basic Energy Sciences, Division of Chemical Sciences. The travel of P.C.D. to Georgia State University was supported by the NSF. A.G.'s work was supported by the Department of Science and Technology, Government of India. The referee's critical comments have helped us significantly improve the manuscript.

[1] M. Ya. Amusia, V. K. Ivanov, and L.V. Chernysheva, Phys. Lett. A **59**, 191 (1976).
[2] V. Radojević, M. Kutzner, and H. P. Kelly, Phys. Rev. A **40**, 727 (1989).
[3] M. Kutzner, Z. Altun, and H. P. Kelly, Phys. Rev. A **41**, 3612 (1990).
[4] H. P. Kelly, S. L. Carter, and B. E. Norum, Phys. Rev. A **25**, 2052 (1982).
[5] U. Becker, D. Szostak, H. G. Kerkhoff, M. Kupsch, B. Langer, R. Wehlitz, A. Yagishita, and T. Hayaishi, Phys. Rev. A **39**, 3902 (1989).
[6] J. M. Bizau, D. Cubaynes, P. Gérard, and F. J. Wuilleumier, Phys. Rev. A **40**, 3002 (1989).
[7] J.-M. Bizau, D. Cubaynes, J.-M. Esteva, F. J. Wuilleumier, C. Blancard, J. Bruneau, J.-P. Champeaux, A. Compant La Fontaine, C. Couillaud, R. Marmoret, C. Rémond, D. Hitz, M. Delaunay, N. Haque, P. C. Deshmukh, H. L. Zhou, and S. T. Manson, Phys. Rev. Lett. **87**, 273002 (2001).
[8] S. B. Whitfield, R. Wehlitz, and V. K. Dolmatov, J. Phys. B **44**, 165002 (2011).
[9] A. Zangwill and P. Soven, Phys. Rev. Lett. **45**, 204 (1980).
[10] U. Fano and J. W. Cooper, Rev. Mod. Phys. **40**, 441 (1969).
[11] A. F. Starace, in *Handbuch der Physik*, edited byW. Mehlhorn (Springer, Berlin, 1982), Vol. 31, pp. 1–121.
[12] W. R. Johnson and C. D. Lin, Phys. Rev. A **20**, 964 (1979).
[13] V. Radojević and W. R. Johnson, Phys. Rev. A **31**, 2991 (1985).
[14] W. R. Johnson and K. T. Cheng, Phys. Rev. A **20**, 978 (1979).
[15] N. Shanthi, P. C. Deshmukh, and S. T. Manson, Phys. Rev. A **37**, 4720 (1988).
[16] G. B. Pradhan, J. Jose, P. C. Deshmukh, V. Radojević, and S. T. Manson, Phys. Rev. A **81**, 063401 (2010).
[17] P. C. Deshmukh and W. R. Johnson, Phys. Rev. A **27**, 326 (1983).
[18] P. C. Deshmukh and S. T. Manson, Phys. Rev. A **28**, 209 (1983).
[19] P. C. Deshmukh, V. Radojević, and S. T. Manson, Phys. Rev. A **45**, 6339 (1992).
[20] H. R. Varma, T. Banerjee, S. Sunil Kumar, P. C. Deshmukh, V. K. Dolmatov, and S. T. Manson, J. Phys. Conf. Ser. **80**, 012025 (2007).
[21] N. Shanthi, J. Phys. B **21**, L427 (1988).
[22] P. Shorer and A. Dalgarno, Phys. Rev. A **16**, 1502 (1977).
[23] V. Radojević and W. R. Johnson, J. Phys. B **16**, 177 (1983).
[24] M. Kutzner and V. Radojević, Phys. Rev. A **49**, 2574 (1994).

[25] P. C. Deshmukh, V. Radojević, and S. T. Manson, Phys. Lett. A **117**, 293 (1986).

[26] C. M. Lee and W. R. Johnson, Phys. Rev. A **22**, 979 (1980).

[27] U. Fano, Nuovo Cimento **12**, 154 (1935).

[28] M. Nrisimhamurty, G. Aravind, P. C. Deshmukh, and S. T. Manson, Phys. Rev. A **91**, 013404 (2015).

[29] F. A. Parpia, C. Froese Fischer, and I. P. Grant, Comput. Phys. Commun. **94**, 249 (1996).

[30] G. B. Pradhan, J. Jose, V. Radojević, S. T. Manson, and P. C. Deshmukh, J. Phys. Conf. Ser. **194**, 022042 (2009).

[31] G. Aarthi, J. Jose, S. Deshmukh, V. Radojević, P. C. Deshmukh, and S. T. Manson, J. Phys. B **47**, 025004 (2014).

[32] J. Jose, G. B. Pradhan, V. Radojević, S. T. Manson, and P. C. Deshmukh, Publ. Astron. Obs. Belgrade **89**, 29 (2010).

[33] J. Jose, G. B. Pradhan, V. Radojević, S. T. Manson, and P. C. Deshmukh, Phys. Rev. A **83**, 053419 (2011).

[34] G. Snell, M. Martins, E. Kukk, W. T. Cheng, and N. Berrah, Phys. Rev A **63**, 062715 (2001).

[35] I. P. Grant, J Phys. B **43**, 074033 (2010).

[36] http://www.nist.gov/pml/data/asd.cfm

[37] A. Derevianko, W. R. Johnson, and K. T. Cheng, At. Data Nuc. Data Tables **73**, 153 (1999).

[38] *Giant Resonances in Atoms, Molecules and Solids*, edited by J. P. Connerade, J. M. Esteva, and R. C. Karnatak, NATO Advanced Study Institute Vol. 151, Series B: Physics (Plenum, New York, 1987).

[39] M. H. Hecht and I. Lindau, Phys. Rev. Lett. **47**, 821 (1981).

[40] S. T. Manson and A. F. Starace, Rev. Mod. Phys. **54**, 389 (1982).

[41] M. Ya. Amusia, Adv. At. Mol. Phys. **17**, 1 (1981), and references therein.

[42] M. Richter, M. Meyer, M. Pahler, T. Prescher, E. V. Raven, B. Sonntag, and H. E. Wetzel, Phys. Rev A, **39**, 5666 (1989).

[43] E. W. B. Dias, H. S. Chakraborty, P. C. Deshmukh, S. T. Manson, O. Hemmers, P. Glans, D. L. Hansen, H. Wang, S. B. Whitfield, D. W. Lindle, R. Wehlitz, J. C. Levin, I. A. Sellin, and R. C. C. Perera, Phys. Rev. Lett. **78**, 4553 (1997).

[44] D. L. Hansen, O. Hemmers, H. Wang, D. W. Lindle, P. Focke, I. A. Sellin, C. Heske, H. S. Chakraborty, P. C. Deshmukh, and S. T. Manson, Phys. Rev. A **60**, R2641(R) (1999).